nature structural & molecular biology

Resolving individual steps of Okazaki-fragment maturation at a millisecond timescale

Joseph L Stodola & Peter M Burgers

DNA polymerase delta (Pol δ) is responsible for elongation and maturation of Okazaki fragments. Pol δ and the flap endonuclease FEN1, coordinated by the PCNA clamp, remove RNA primers and produce ligatable nicks. We studied this process in the *Saccharomyces cerevisiae* machinery at millisecond resolution. During elongation, PCNA increased the Pol δ catalytic rate by >30-fold. When Pol δ invaded double-stranded RNA–DNA representing unmatured Okazaki fragments, the incorporation rate of each nucleotide decreased successively to 10–20% that of the preceding nucleotide. Thus, the nascent flap acts as a progressive molecular brake on the polymerase, and consequently FEN1 cuts predominantly single-nucleotide flaps. Kinetic and enzyme-trapping experiments support a model in which a stable PCNA–DNA–Pol δ–FEN1 complex moves processively through iterative steps of nick translation, ultimately completely removing primer RNA. Finally, whereas elongation rates are under dynamic dNTP control, maturation rates are buffered against changes in dNTP concentrations.

In eukaryotes, Okazaki-fragment synthesis is initiated by DNA polymerase (Pol) α–primase, which creates a 20- to 30-base primer initiated by approximately 7–10 nt of RNA[1]. A conserved and highly regulated process synthesizes lagging-strand DNA from these primers and removes the Pol α–primase–synthesized RNA from each of the ~50 million Okazaki fragments synthesized in mammalian cells, forming continuous double-stranded DNA upon nick ligation[2]. Many different DNA structures are formed during Okazaki-fragment synthesis and maturation, and improper processing of these intermediates is a major cause of genome instability. Moreover, mutations can arise from the incomplete removal of Pol α–synthesized DNA[3].

Pol δ performs the bulk of lagging-strand DNA synthesis, extending Pol α primers until reaching the 5′ terminus of the preceding Okazaki fragment. In *S. cerevisiae*, Pol δ is a three-subunit complex consisting of Pol3, Pol31, and Pol32 (ref. 4). The catalytic subunit, Pol3, contains both the polymerase and the proofreading 3′–5′ exonuclease activities. Each subunit contains motifs that bind to the sliding clamp proliferating cell nuclear antigen (PCNA)[4–8]. When loaded onto primer termini by replication factor C (RFC) in an ATP-dependent reaction[9], PCNA increases the intrinsic processivity of Pol δ, allowing it to replicate hundreds of nucleotides in a single DNA binding event[10].

Because Okazaki fragments are initiated with Pol α–synthesized RNA, ligation cannot occur until initiator RNA is removed. This removal requires the joint activity of Pol δ and the structure-specific flap endonuclease I (FEN1). When Pol δ reaches the 5′ end of the previous Okazaki fragment, it continues replicating by limited displacement of the RNA primer, forming a 5′ flap, which is cut by FEN1. To completely remove the RNA primer, it has been proposed that iterative Pol δ strand displacement and FEN1 cleavage is required, a process termed nick translation[11,12]. The forward movement of Pol δ that results in strand displacement is countered by exonucleolytic activity of Pol δ, which reverses this action; repetition of this cycle is known as idling. Idling supports maintenance of the nick position in the absence of other processing activities[13]. Without idling, unregulated strand-displacement synthesis generates problematic long flaps that require alternative processing mechanisms[14] and can cause lethality when FEN1 activity is also compromised[15].

Okazaki-fragment maturation, involving the action of Pol δ, FEN1, and DNA ligase I, is the best-studied example of a sequential multienzyme process coordinated by PCNA. For maturation to occur efficiently, cooperation with PCNA must be tightly regulated, and enzymes exchange access for DNA intermediates in a prescribed sequence. Debate remains concerning the mechanism of this cooperation. Because of PCNA's homotrimeric structure, it has been suggested that multiple enzymes may simultaneously bind to PCNA, each occupying a separate monomer; this is called the tool-belt model[16]. Biochemical evidence in support of tool-belt models has been reported in bacterial systems[16,17] and in archaea[18]. The alternative model presupposes dynamic binding to and dissociation from PCNA, thus resulting in sequential switching of partners. Use of engineered yeast PCNA heterotrimers has provided biochemical evidence that nick translation does not absolutely require simultaneous binding of Pol δ and FEN1 (ref. 19), but the methodology has not allowed for evaluation of whether this switching actually occurs.

Although the general pathway of Okazaki-fragment maturation has been well established, several critical mechanistic steps have remained unresolved because of the low kinetic resolution of existing studies. With the goal of better understanding how PCNA coordinates multiple enzymes during Okazaki-fragment synthesis and maturation, we

Department of Biochemistry and Molecular Biophysics, Washington University School of Medicine, Saint Louis, Missouri, USA. Correspondence should be addressed to P.M.B. (burgers@biochem.wustl.edu).

Received 18 December 2015; accepted 18 March 2016; published online 11 April 2016; corrected online 19 April 2016 (details online); doi:10.1038/nsmb.3207

performed millisecond-resolution kinetic studies with a quench-flow apparatus. This analysis reveals new and unexpected insights into the regulation of 5′-flap generation and processing. Furthermore, our analysis provides evidence for the proposed tool-belt model of the Okazaki-fragment maturation machinery.

RESULTS

PCNA increases the catalytic rate of Pol δ

The experimental design of our studies in the quench-flow apparatus is described in Online Methods. Unless otherwise noted, the exonuclease-deficient Pol δ-DV was used in all experiments to prevent degradation of DNA substrates[15]. We started by measuring the rate of incorporation of a single nucleotide by a preformed DNA–Pol δ complex (**Fig. 1a**); this rate constant is $9 \pm 1\ s^{-1}$ (**Fig. 1b**,**c**). Under our standard assay conditions, binding of the polymerase to DNA was saturated, and the dTTP concentration (250 μM) was near saturation (**Supplementary Fig. 1a**,**b**). This rate constant was higher than that observed in a previous analysis of Pol δ (ref. 20) but much slower than previously determined rates of replication by PCNA–Pol δ on RPA-coated single-stranded DNA[21]. We first investigated whether inclusion of RPA enhanced the catalytic rate of Pol δ alone, and we found instead that RPA strongly inhibited incorporation (**Supplementary Fig. 1e**).

In contrast, when PCNA was loaded onto DNA, we observed that PCNA–Pol δ incorporated a single nucleotide at a rate too fast to be accurately determined in our apparatus (>300 s^{-1}) (**Fig. 1b**,**c**). Because polymerase was prebound to DNA in both experiments, the increase in the rate constant was probably caused by intrinsic stimulation of the nucleotide incorporation rate by PCNA. Whether PCNA enhances the rate of the conformational change of the ternary polymerase–DNA–dNTP complex or the chemical step cannot be distinguished here[22]. Nevertheless, these data provide evidence that PCNA can actively influence the catalytic activity of a bound enzyme in addition to stabilizing it on DNA.

To determine how RPA influenced the rate of nucleotide incorporation by PCNA–Pol δ, we initiated reactions with dTTP and dATP, allowing the polymerase to incorporate 21 nt (**Fig. 1a**,**d** and **Supplementary Fig. 1d**). For graphical representation, we plotted the median extension product as a function of time (**Fig. 1e** and description of analysis in Online Methods). At saturating dNTP concentrations (**Supplementary Fig. 1c**), PCNA–Pol δ synthesized at a rate of ~340 nt/s, with or without RPA (**Fig. 1e**), thus indicating that RPA does not affect replication of homopolymeric templates. On mixed-sequence DNAs, RPA aids in processivity by resolving secondary structures; however, this stimulation can also be accomplished by heterologous single-stranded binding proteins[23,24].

In yeast, dNTP concentrations are only 12–30 μM (ref. 25). When we performed extension reactions with physiological levels of the four dNTPs, replication rates were reduced substantially, to 66 nt/s, thus indicating that these rates are not maximized at normal cellular dNTP levels (**Supplementary Fig. 1f**,**g**). These submaximal rates are advantageous for fidelity purposes because proofreading of errors is more efficient at subsaturating dNTP concentrations[26]. Furthermore, rNTPs, which are present at much higher concentrations than dNTPs, represent a discrimination challenge to DNA polymerases[25,27]. When we included both dNTPs and rNTPs at physiological concentrations, DNA synthesis by PCNA–Pol δ proceeded at a rate of 51 nt/s (**Supplementary Fig. 1f**,**g**), a rate compatible with rates of fork movement in yeast[28].

Strand-displacement synthesis by Pol δ

We next observed Pol δ approaching the 5′ terminus of a model Okazaki fragment and initiating strand-displacement synthesis. Previous experiments have lacked the kinetic resolution to determine what occurs when Pol δ reaches the double-stranded block and which features of the 5′ block determine the kinetics of this process[21,29]. We annealed the primer and a downstream oligonucleotide block to their

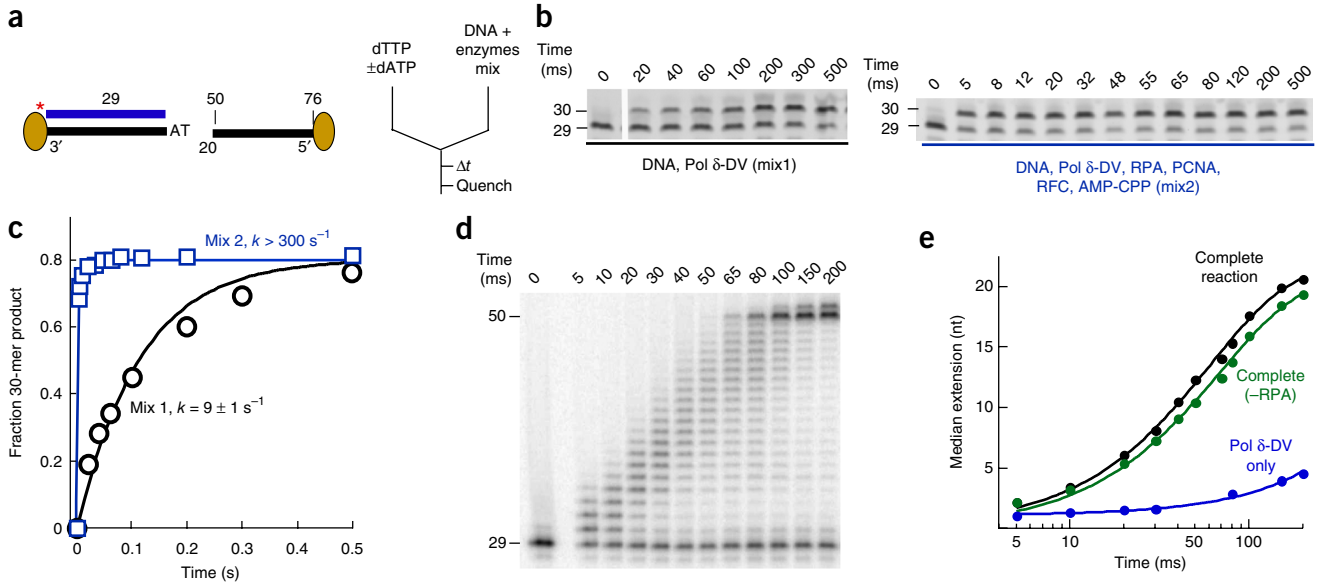

Figure 1 PCNA stimulates the catalytic rate of Pol δ. (**a**) DNA substrate and rapid-quench experimental setup. Asterisk indicates position of label. (**b**) Time courses of single-nucleotide incorporation by Pol δ-DV. Reactions contained standard DNA and enzyme concentrations, as described in Online Methods, with or without accessory proteins as defined in 'mixes'. Reactions were initiated with 250 μM dTTP. (**c**) Quantification of data in **b**. Time courses were fit to single exponentials, representative of first-order kinetics (mean ± s.d.). (**d**) Replication of a homopolymeric DNA by PCNA–Pol δ. Reactions contained all accessory proteins and were initiated with 250 μM of each dTTP and dATP, allowing extension of 29-mer to a 50-mer product. (**e**) Quantification of data in **d** and of **Supplementary Figure 1d**. Median extension was determined as described in detail in Online Methods. Black, complete reaction containing DNA and Pol δ-DV, RPA, PCNA, RFC, and AMP-CPP; green, reaction containing all components except RPA; blue, reaction containing only DNA and Pol δ-DV.

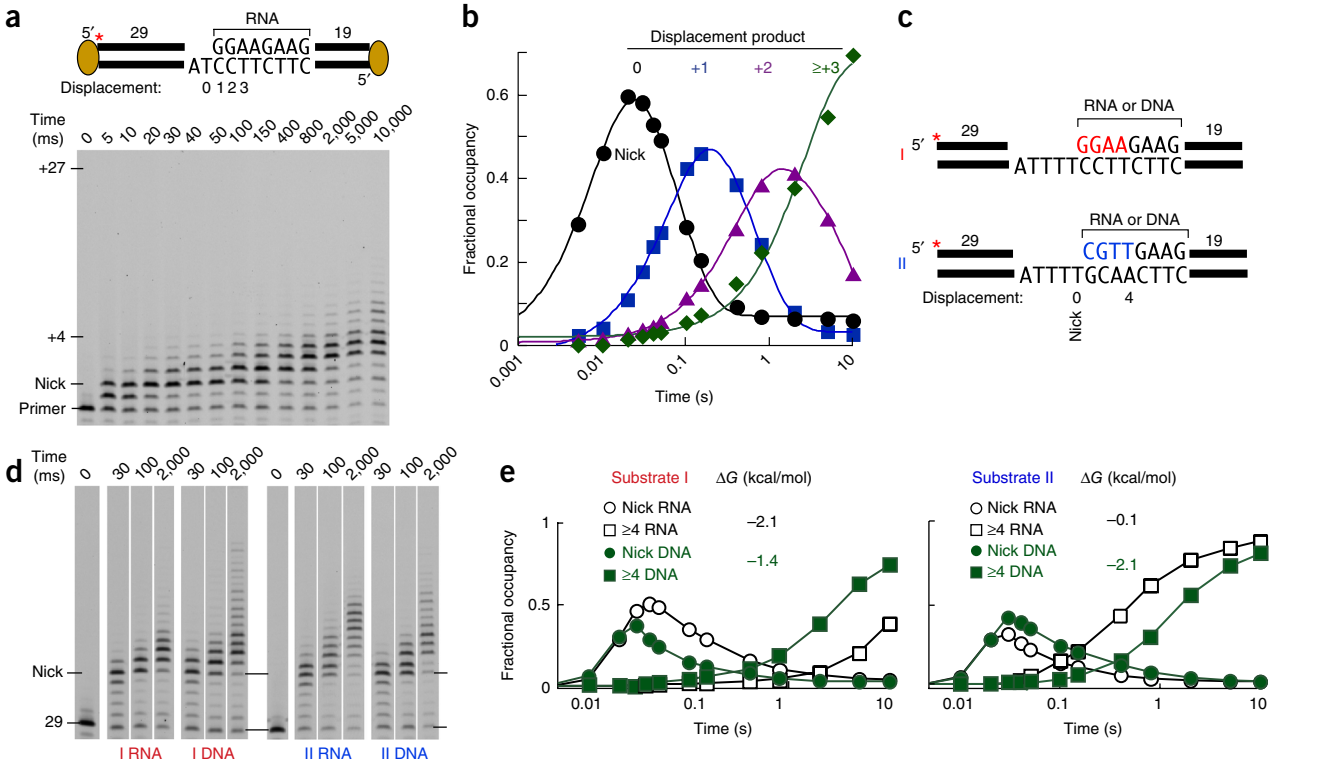

Figure 2 Strand-displacement synthesis by PCNA–Pol δ. (**a**) Top, model of DNA substrate. Strand-displacement positions (nick = 0) are indicated. Block was initiated with RNA_8. Bottom, gel of replication products. Asterisk indicates position of label. (**b**) Quantification of data in **a**. Fractional occupancy of strand-displacement intermediates. Nick position (circles), and strand-displacement products of one (squares), two (triangles), and three or more (diamonds) nucleotides are shown. Time courses were fit to the sum of two exponentials, to model formation and decay of intermediates, with the exception of the ≥+3 (green) curve, which was fit to a single exponential. (**c**) Strand-displacement substrates used in **d**, containing a 5-nt gap. Substrate I (red) and substrate II (blue) differ in four nucleotides at the 5′ end of the blocking oligonucleotide. Blocks were initiated with either RNA_8 or DNA_8 as indicated. Asterisks indicate position of label. (**d**) Select time points of strand-displacement time courses; full time courses are shown in **Supplementary Figure 2c**,**d**. (**e**) Fractional occupancy of select replication products from **d**. Nick position (circles) and intermediates four nucleotides or more past the nick (squares) are plotted. Free-energy (Δ*G*) values of the 5′-terminal 4-bp duplexes were calculated as previously described[30].

corresponding templates (**Fig. 2a**,**c**), leaving either a 2-nt or a 5-nt gap between the primer terminus and block.

We first focused on the substrate with a 2-nt gap and a RNA_8DNA_{19} block (**Fig. 2a**). We performed rapid-quench kinetic experiments with the complete system (RPA, PCNA, RFC, Pol δ-DV, and α,β-methyleneadenosine 5′-triphosphate (AMP-CPP), as described in **Fig. 1a**) but in the presence of all four dNTPs at saturation. After reaction initiation with dNTPs, Pol δ rapidly extended the primer at 200–300 nt/s. We plotted the fractional occupancy of the nick product and of each strand-displacement product over time (**Fig. 2b**). The final nucleotide closing the gap into a nick was inserted at a rate ~50% that of the normal synthesis rate, thus indicating that the presence of the block is sensed by the polymerase. Pol δ stalled substantially at the nick position (designated as 0), thus indicating that it cannot seamlessly initiate strand displacement. Furthermore, the observed rate of nucleotide incorporation, in which the polymerase invaded the duplex DNA, slowed to 10–20% that of the previous step, from 11.3 ± 1.0 s^{-1} for the first nucleotide displaced, to 1.4 ± 0.2 s^{-1} for the second, to 0.38 ± 0.06 s^{-1} for the third nucleotide. Thus, the nascent flap acts as a progressive molecular brake on the DNA polymerase, limiting formation of longer flaps. Furthermore, this progressive slowdown was not the result of specific DNA or RNA sequences but instead was a consequence of the increasing length of the flap (**Supplementary Fig. 2e–g**). To extend the model-free fitting in **Figure 2b**, we performed global kinetic fitting of these data to two different models. These models are discussed in detail in **Supplementary Fig. 2a**,**b** and their implications are considered further in the Discussion.

Given its function in Okazaki-fragment maturation, Pol δ may have evolved the ability to displace RNA–DNA duplexes more readily than DNA–DNA duplexes. We investigated whether either the duplex stability or the sugar identity (RNA versus DNA) is the main determining factor for strand-displacement capacity. We focused on the relative duplex stabilities of the 5′-proximal 4 bp that initially block invasion by Pol δ (**Fig. 2c**). RNA–DNA and DNA–DNA duplex stabilities have been determined by nearest-neighbor analysis[30]. The RNA–DNA duplex of substrate I was more stable than the DNA–DNA duplex by 0.7 kcal/mol. Pol δ reached the nick at the same rate for both substrates (**Fig. 2d**,**e** and **Supplementary Fig. 2c**). However, the rate of release from the nick position and strand-displacement synthesis proceeded faster for the DNA–DNA duplex than for the more stable RNA–DNA duplex. When we reversed the duplex stabilities, with the DNA–DNA substrate being more stable, the RNA block was displaced more rapidly than the DNA block (**Fig. 2c–e** and **Supplementary Fig. 2d**). These data suggest that strand-displacement rates are governed primarily by duplex stability rather than by RNA versus DNA identity.

Pol δ idling at a nick

We carried out the studies above with exonuclease-deficient Pol δ-DV, so that calculations of forward polymerization rates were uncomplicated by exonucleolytic degradation. After limited strand displacement,

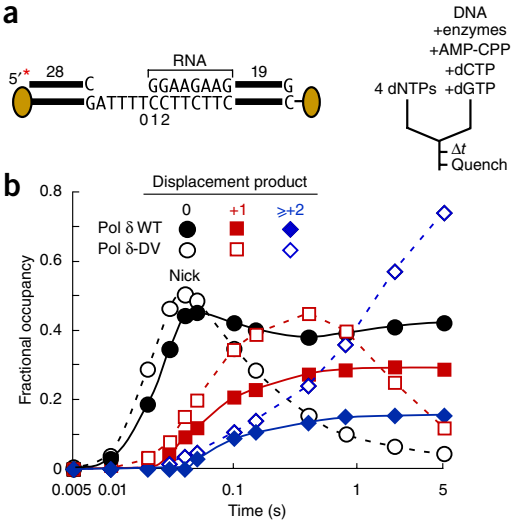

Figure 3 Strand-displacement synthesis and idling by wild-type Pol δ. (**a**) DNA substrate I. RNA block was preincubated with RPA, PCNA, RFC, AMP-CPP, and Pol δ under standard assay conditions, with 150 μM dCTP and dGTP to prevent degradation of oligonucleotides by wild-type Pol δ. Asterisk indicates position of label. (**b**) Distribution of strand-displacement products of Pol δ-DV and wild-type (WT) Pol δ. Quantification of data in **Supplementary Figures 3a** (wild type) and **2c** (DV). Fractional occupancies of the nick position, +1 product, and +2 or more products past the nick are plotted.

wild-type Pol δ degrades DNA back to the nick position, using its exonuclease in a process called idling[13]. To perform experiments with wild-type Pol δ, we assembled replication-competent complexes in the presence of dCTP and dGTP to prevent substrate degradation, and we initiated replication by addition of the four dNTPs (**Fig. 3a**). We compared fractional occupancies of select replication intermediates with those measured with Pol δ-DV (**Fig. 3b** and **Supplementary Fig. 3a**). Replication up to the nick position was comparable for both forms of Pol δ. However, as the wild-type enzyme invaded the nick, it reversed, using its exonuclease activity. As a result, the fraction of nick products did not decay, and in comparison with the results for Pol δ-DV, flap products did not accumulate (**Fig. 3b**). An equilibrium distribution of products maintained by idling was reached within 500 ms. At equilibrium, the fractional occupancy of nick product was comparable to that of all flap products combined, thus suggesting that the rate of degradation was comparable to that of strand displacement of the first nucleotide (~10 s^{-1}). Rates of strand displacement by wild-type Pol δ were also governed by the stability of the block. A more stable block yielded an equilibrium distribution of extension products favoring the nick product and shorter flaps (**Supplementary Fig. 3b–d**).

FEN1 processes single-nucleotide flaps

We next reconstituted nick-translation synthesis, which requires coordinated action of Pol δ and FEN1. Structural and mechanistic studies have shown that FEN1 does not simply cut 5′ flaps at their base, as generally depicted, but binds a single 3′ extrahelical nucleotide into a specificity pocket, then cuts the 5′ strand one nucleotide into the double-stranded DNA, which itself has become partially unpaired[31]. For a single-nucleotide 5′ flap, which can equilibrate into a 3′ flap, the proposed cleavage mechanism is depicted in **Figure 4a**. Previous studies have shown that the major product produced by FEN1 during nick translation is a mononucleotide[12], which is presumably the result of cleavage following formation of a 1-nt flap by Pol δ. However, many studies have shown that the 1-nt flap is not the preferred substrate for FEN1; instead, FEN1 cuts double-flap structures with a single-nucleotide 3′ flap and a variable-length 5′ flap much more avidly[31–33]. Indeed, in our sequence context, double-flap substrates were cut faster than the single nucleotide flap (**Supplementary Fig. 4i**). Given the temporal resolution of our system, we were able to determine which strand-displacement products provide substrates for FEN1. We labeled DNA substrates in various positions (**Fig. 4b**) to monitor different enzyme activities. Then we initiated reactions with dNTPs together with FEN1 (**Fig. 4b**). Addition of FEN1 did not alter the rate at which Pol δ reached the nick position or the rate of +1 extension-product formation (**Fig. 4b** and **Supplementary Fig. 4a**,**b**). However, the addition of FEN1 led to a very rapid decay of the +1 extension product, thus suggesting that FEN1 acted on this substrate (**Fig. 4c**).

We also monitored the production of FEN1-digestion products. The mononucleotide product predominated, but dinucleotides and trinucleotides were also formed (**Supplementary Fig. 4c**). The 1-nt cleavage product formed with kinetics that lagged behind the formation of the +1 displacement product but preceded formation of the +2 displacement product (**Fig. 4c**), thus indicating that the 1-nt cleavage product resulted from the displacement of a single nucleotide. If reequilibration of the single-nucleotide 5′ flap into a 3′ flap is a prerequisite for FEN1 activity, reequilibration must occur at a timescale faster than cutting (>5 s^{-1}). Products of 2 nt and 3 nt resulted from processing of longer flaps that accumulated at later times (**Supplementary Fig. 4d**). Efficient flap cleavage relied on the interaction between PCNA and FEN1. The PCNA-defective mutant FEN1-p[34] was strongly compromised in cutting flaps generated by PCNA–Pol δ (**Fig. 4d** and **Supplementary Fig. 5e**).

The prediction from these studies is that relative rates of strand-displacement synthesis through sequences with different stabilities determine the distribution of FEN1 products. This is indeed what we observed; on our most stable substrate (substrate III), strand-displacement synthesis proceeded much more slowly than on the standard substrate (**Supplementary Fig. 2f**,**g**), and FEN1 products longer than the mononucleotide were negligible (**Supplementary Fig. 4e–g**). From these data sets, we conclude that the major FEN1 substrate during nick translation is a single-nucleotide flap and not the double flap that is more active in FEN1 cutting.

Coupling strand displacement to FEN1 action

A central proposal in the current view of nick translation is its coupled, reiterative nature, i.e., that multiple cycles of strand displacement and FEN1 cutting of predominantly 1-nt flaps removes the initiator RNA. As such, we predict that first, FEN1 cuts iteratively at every position in the downstream oligonucleotide, in effect producing a ladder of products, and second, the degradation of the downstream oligonucleotide should match the extension of the primer oligonucleotide. To visualize all intermediates of FEN1 cutting, we labeled the 3′ end of the blocking oligonucleotide (**Fig. 4b**). Indeed, we observed a ladder of downstream oligonucleotides resulting from regular and reiterative FEN1 cutting. To examine polymerase–FEN1 coupling, we compared the median primer length of products replicated past the nick position with the median length of 3′-labeled oligonucleotides cut by FEN1 (**Fig. 4b**,**e**). When plotted, the slopes were nearly equivalent, with the median primer length increasing at ~5 nt/s and the median downstream oligonucleotide degrading at ~4 nt/s. This inverse relationship suggests a tight coupling of strand displacement and FEN1 nuclease activity during nick translation.

If polymerization during nick translation were rate limiting, a decrease in dNTP concentrations from saturating to physiological

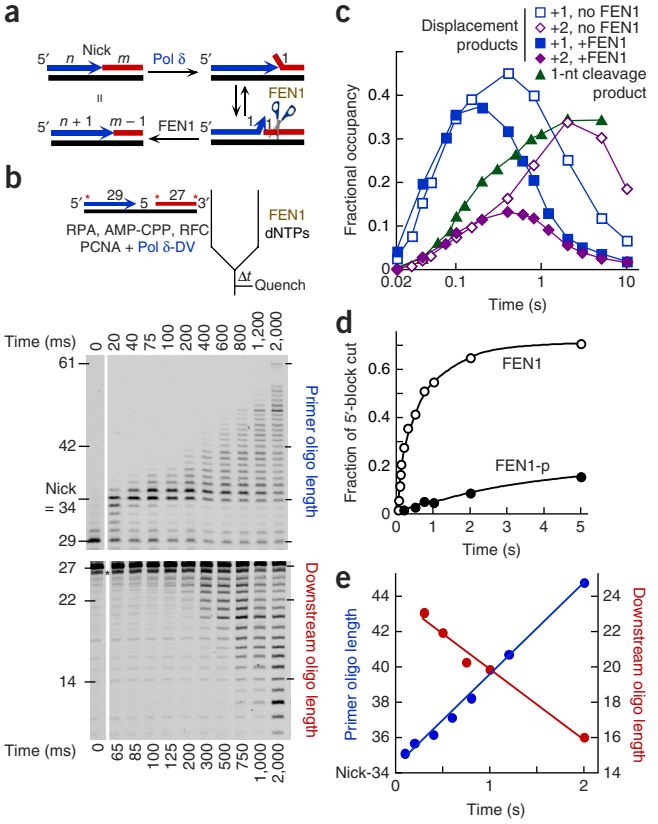

Figure 4 Nick translation by Pol δ and FEN1. (**a**) Model for the FEN1 mechanism in nick translation *n* and *m* are arbitrary DNA lengths. (**b**) Top, design of the nick translation assay. DNA templates (substrate I RNA block) contained a 5′-primer label, a 5′-block label, or a 3′-block label. 5′-primer labeling reports extension by Pol δ. 5′-block labeling measures the first product released by FEN1. 3′-block labeling measures how far FEN1 has cut into the block. The PCNA–Pol δ complex was preformed, and reactions were initiated with dNTPs plus 40 nM FEN1. Top gel, primer extension (5′-labeled primer); bottom gel, FEN1 cleavage of block (3′-labeled block). Asterisk, nonspecific band; oligo, oligonucleotide. (**c**) Quantification of data in **b** (top gel, +FEN1), **Supplementary Figure 2c** (substrate I RNA, no FEN1), and **Supplementary Figure 4c** (fraction of 1-nt product). (**d**) 5′-labeled-block products cut by FEN1 or FEN1-p (40 nM). Fraction cut is the sum of 1-, 2-, and 3-nt products. (**e**) Quantification of data in **b**. Blue, median extension product past the nick position (left *y* axis) derived from the top gel; red, median cleavage product (right *y* axis) derived from the bottom gel. Analysis of the FEN1-generated products (bottom gel) was started at the 300-ms time point, at which substantial FEN1-mediated degradation had occurred. Asterisk denotes the presence of contaminants in the oligonucleotide, which precluded accurate quantification of products at earlier time points.

levels should decrease the nick-translation rate to ~25%, as observed with unimpeded elongation (**Supplementary Fig. 1g**). We performed nick translation assays at physiological dNTP concentrations. Primer-elongation rates during the linear range of nick translation were comparable at both saturating and physiological dNTP concentrations (**Supplementary Fig. 4h**), thus indicating that other steps during nick translation are likely to be rate limiting.

Experimental evaluation of the PCNA tool-belt model

Interaction with PCNA allows Pol δ to replicate single-stranded DNA processively, but the extent to which PCNA–Pol δ can perform processive strand-displacement synthesis, and whether a stable PCNA–Pol δ–FEN1 complex exists that performs processive nick translation, remains unresolved. To determine whether PCNA–Pol δ can processively replicate through a typical Okazaki-fragment primer (~7–10 nt), we used heparin to trap free Pol δ that had dissociated from DNA (**Fig. 5a**). In the absence of PCNA, 10 μg/ml heparin completely inhibited Pol δ even when the polymerase was prebound to DNA (**Fig. 5a**, lanes 1 and 2). A second control experiment showed that pretrapped Pol δ could not bind PCNA–DNA, and replication was inhibited (lanes 9 and 10). However, when Pol δ was prebound to PCNA–DNA, challenge with heparin upon initiation with dNTPs did not cause a decrease in strand-displacement products after 5 s, and we observed only a partial decrease after 20 s (lanes 3–6), thus indicating

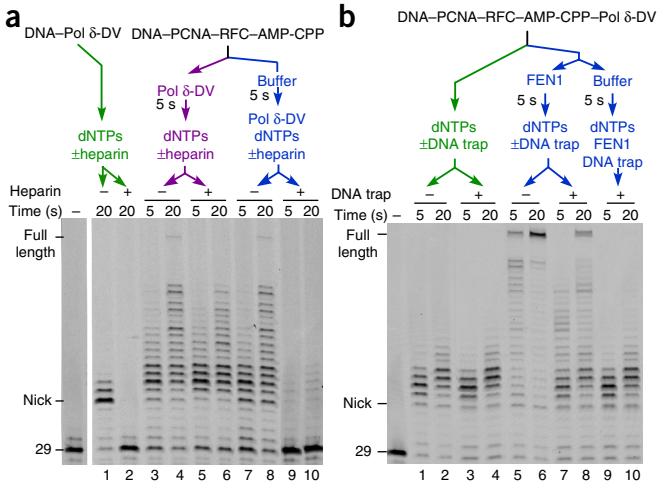

that the complex is processive at the timescale during which nick translation normally occurs. Processive strand-displacement synthesis occurred through either DNA or RNA blocks, and at saturating or physiological dNTP levels (**Fig. 5a** and **Supplementary Fig. 5a**,**b**).

Second, we asked whether FEN1 also acted processively during nick translation. Because heparin inhibited FEN1 under all conditions (data not shown), we used an oligonucleotide-trap substrate with a structure representing the optimal substrate for FEN1 (**Supplementary Fig. 5e**). This trap did not inhibit strand-displacement synthesis by Pol δ (**Fig. 5b**, lanes 1–4). In a control experiment, when FEN1 was prebound to the oligonucleotide trap before reaction initiation with dNTPs, we observed no products longer than the expected strand-displacement products (lanes 3 and 4 and 9 and 10), thus indicating that the trap did not inhibit strand-displacement synthesis but did inhibit FEN1. In addition, preincubation of FEN1 with the trap blocked cleavage of a preformed flap-containing DNA (**Supplementary Fig. 5e**). However, when FEN1 was allowed to assemble onto the DNA–PCNA–Pol δ complex before addition of dNTPs with the DNA trap, very long extension products were formed, consistently with FEN1 acting processively during multiple cycles of nick translation (**Fig. 5b**, lanes 5 and 6 and 7 and 8). The processivity of nick translation was not absolute, because more efficient nick translation was observed in the absence of the trap, which allowed reloading of dissociated FEN1. One caveat of this experiment is that,

Figure 5 Processivity of the nick-translation machinery. (**a**) Strand-displacement synthesis by PCNA–Pol δ on the substrate I DNA block. Reactions were initiated with 250 μM dNTPs with or without 10 μg/ml heparin. (**b**) Nick translation assay; forced single turnover of 40 nM FEN1. The DNA template was substrate I RNA block. Reactions were initiated with 250 μM dNTPs, with or without 6 μM oligonucleotide FEN1 trap (**Supplementary Fig. 4i**, bottom DNA).

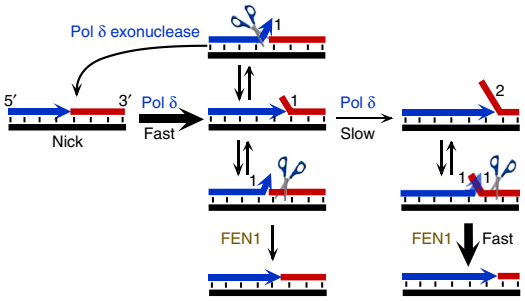

Figure 6 Model for short-flap maintenance and nick translation. Details are in main text.

because the DNA trap does not trap Pol δ, we formally cannot exclude the possibility that some polymerase dissociated and rebound during nick translation, even while FEN1 remained bound. However, because FEN1 remained processive, a DNA–PCNA–Pol δ–FEN1 complex that advances nick translation must exist.

These processive activities are completely dependent on the interaction of FEN1 with PCNA, because they were abrogated when we used the PCNA-interaction-defective mutant FEN1-p (**Supplementary Fig. 5c**). Stable FEN1 binding to PCNA during nick translation did not depend on the form of polymerase used, because both exonuclease-deficient Pol δ-DV and wild-type Pol δ showed processive nick translation (**Fig. 5b** and **Supplementary Fig. 5d**). In sum, these data provide evidence that the quaternary DNA–PCNA–Pol δ–FEN1 complex performs efficient and processive nick translation.

DISCUSSION

Our high-resolution kinetic analysis has illuminated new aspects of the basic steps of Okazaki-fragment synthesis and maturation. Analysis of the DNA–Pol δ complex yielded the unexpected result that the presence of PCNA greatly accelerated the observed incorporation rate of Pol δ (**Fig. 1**). This finding was surprising because the leading-strand Pol ε shows a high rate of incorporation in the absence of PCNA (~200–300 nt/s), which is comparable to that of PCNA–Pol δ (ref. 35). Furthermore, the orthologous bacteriophage T4 DNA polymerase shows a full catalytic rate of ~400 s^{-1} in the absence of its PCNA-like replication clamp[36]. Thus, Pol δ shows two unique PCNA-stimulated activities: catalysis and processivity.

Our analysis focused on strand-displacement synthesis by Pol δ and on nick translation, to determine which activities could act in synergy to restrict flap sizes. When the polymerase enters an RNA–DNA or DNA–DNA block and initiates strand-displacement synthesis, a progressive molecular brake is applied to the polymerase. Reduction of base-pairing energetics at the block alleviates the severity of the molecular brake. We show here that this alleviation can be accomplished by introducing less stable sequences at the block site (**Fig. 2**), but it can also be accomplished by reducing the salt concentration or raising the assay temperature[21], or even by mechanically pulling on the displaced strand, as shown by single-molecule techniques[37].

Our modeling of the kinetics of strand-displacement synthesis does not currently allow us to conclusively provide a specific molecular mechanism explaining the progressive slowing of the polymerase. We considered two different models in **Supplementary Figure 2a**,**b**. It is possible that nucleotide insertion by Pol δ is progressively inhibited by the growing flap (model 1), or that during strand-displacement synthesis, the enzyme equilibrates between an extension-competent form and an extension-incompetent form (model 2), or that a combination of both models occurs. Model 1 does not sufficiently describe our data because it does not contain steps in which Pol δ switches from its polymerase to its exonuclease domain (idling, **Fig. 3**) or steps in which the primer terminus is released, thus allowing FEN1 to act (nick translation, **Fig. 4**). Even though several rates in model 2 remain poorly defined, we believe that this model has merit because it incorporates these additional steps necessary for nick translation.

Several studies, including ours (**Supplementary Fig. 4i**), have indicated that the 1-nt flap is not the optimal FEN1 substrate[31,33]. Yet this structure is cut most frequently because it is the substrate presented to FEN1 during nick translation; the rate with which the 2-nt flap is produced from the 1-nt flap is generally lower than that of FEN1 cutting (**Fig. 4c**). However, if 2-nt or longer flaps are made, albeit infrequently, the increased rate with which they are cut by FEN1 should ensure that flaps generally do not grow to a dangerously long size (**Fig. 6**).

PCNA's homotrimeric structure has the potential to serve as a binding platform for multiple enzymes simultaneously (the tool-belt model). Previous studies have shown that two functional PCNA monomers are sufficient for full Pol δ activity[19]. Because FEN1 binds only a single PCNA monomer[38], Pol δ and FEN1 have the potential to remain simultaneously bound to a single PCNA during nick translation. Our data support the model in which a quaternary DNA–PCNA–Pol δ–FEN1 complex performs processive nick-translation synthesis. Evaluating the PCNA tool-belt model *in vivo* remains a challenge. The PCNA interaction defect in FEN1-p not only reduced nuclease recruitment to the emerging flap but also prevented processive action by FEN1 during nick translation (**Supplementary Fig. 5c**). The latter defect prevents the tool-belt mechanism from operating. Remarkably, despite these defects, FEN1-p (*rad27-p*) mutants show only marginal genetic instability phenotypes in yeast[34,39]. However, when redundant controls on excessive strand-displacement synthesis are eliminated, such as in a Pol δ exonuclease–defective mutant, the *rad27-p* mutation can cause synthetic lethality[40]. At this point, we are unable to attribute the genetic defect of the *rad27-p* mutant to either the recruitment or processivity defect of FEN-p.

We show that Pol δ processively performs strand displacement on a timescale relevant for Okazaki-fragment maturation (**Fig. 5a**); nick translation proceeds at a rate of ~5 nt/s (**Fig. 4e**), thus suggesting that removal of RNA should generally be accomplished within 2 s. A previous report has determined that Pol δ collision with the 5′ end of an Okazaki fragment decreases the affinity of the polymerase for DNA, designated 'collision release'[24]. Because we found that the whole process should be complete within just a few seconds, our data do not disagree with those from that study, which was carried out on a time scale of minutes. Therefore, although the collision release model may be important under some circumstances, appreciable dissociation of Pol δ occurs too slowly to substantially affect nick translation. It could be argued that at lower, physiological dNTP concentrations, nick translation might occur at a reduced rate. However, we found this not to be the case (**Supplementary Fig. 4h**). These data suggest that steps other than primer elongation are rate limiting; these steps are likely to involve the consecutive steps of polymerase release, flap reequilibration, FEN1 flap engagement, and cutting. Nucleotide levels in yeast are under dynamic control, for example, during the stress response[41]. Our data suggest that, whereas elongation rates are under strict dNTP control, maturation rates are buffered against changes in dNTP concentrations.

The focus of our study has been on Pol δ and FEN1, and their DNA-bound complex with PCNA. DNA ligase I, which completes the process, was not included in this study. In archaeal replication studies, a processive complex of polymerase, FEN1, and ligase with the heterotrimeric PCNA has been observed[18,42]. It is likely that the eukaryotic machinery works in a slightly different manner. Eukaryotic

DNA ligase I also contains a PCNA-binding domain[43], one function of which is recruiting ligase to replication foci[44]. However, previous studies have shown that ligase acts distributively, and the position of ligation after RNA removal is largely dependent on ligase concentrations[21]. In yeast, acute depletion of DNA ligase allows nick translation to proceed up to the dyad of the nucleosome that has been assembled on the completed lagging strand[45]. The analysis of these small fragments has provided valuable information regarding the limits that the cellular environment sets to nick translation by the PCNA–Pol δ–FEN1 complex.

METHODS

Methods and any associated references are available in the online version of the paper.

Note: Any Supplementary Information and Source Data files are available in the online version of the paper.

ACKNOWLEDGMENTS

The authors thank J. Majors, R. Galletto, and T. Lohman for critical discussions during the progress of this work, and C. Stith for protein purification. This work was supported in part by the US National Institutes of Health (GM032431 to P.B.) and from the US-Israel Binational Science Foundation (2013358 to P.B.).

AUTHOR CONTRIBUTIONS

J.L.S. and P.M.B. designed experiments and analyzed data. J.L.S. performed all experiments. J.L.S. and P.M.B. wrote the manuscript.

COMPETING FINANCIAL INTERESTS

The authors declare no competing financial interests.

1. Perera, R.L. *et al.* Mechanism for priming DNA synthesis by yeast DNA polymerase α. *eLife* **2**, e00482 (2013).
2. Balakrishnan, L. & Bambara, R.A. Eukaryotic lagging strand DNA replication employs a multi-pathway mechanism that protects genome integrity. *J. Biol. Chem.* **286**, 6865–6870 (2011).
3. Reijns, M.A. *et al.* Lagging-strand replication shapes the mutational landscape of the genome. *Nature* **518**, 502–506 (2015).
4. Gerik, K.J., Li, X., Pautz, A. & Burgers, P.M. Characterization of the two small subunits of *Saccharomyces cerevisiae* DNA polymerase delta. *J. Biol. Chem.* **273**, 19747–19755 (1998).
5. Bermudez, V.P., MacNeill, S.A., Tappin, I. & Hurwitz, J. The influence of the Cdc27 subunit on the properties of the *Schizosaccharomyces pombe* DNA polymerase delta. *J. Biol. Chem.* **277**, 36853–36862 (2002).
6. Lu, X. *et al.* Direct interaction of proliferating cell nuclear antigen with the small subunit of DNA polymerase delta. *J. Biol. Chem.* **277**, 24340–24345 (2002).
7. Netz, D.J. *et al.* Eukaryotic DNA polymerases require an iron-sulfur cluster for the formation of active complexes. *Nat. Chem. Biol.* **8**, 125–132 (2012).
8. Acharya, N., Klassen, R., Johnson, R.E., Prakash, L. & Prakash, S. PCNA binding domains in all three subunits of yeast DNA polymerase δ modulate its function in DNA replication. *Proc. Natl. Acad. Sci. USA* **108**, 17927–17932 (2011).
9. Tsurimoto, T. & Stillman, B. Functions of replication factor C and proliferating-cell nuclear antigen: functional similarity of DNA polymerase accessory proteins from human cells and bacteriophage T4. *Proc. Natl. Acad. Sci. USA* **87**, 1023–1027 (1990).
10. Chilkova, O. *et al.* The eukaryotic leading and lagging strand DNA polymerases are loaded onto primer-ends via separate mechanisms but have comparable processivity in the presence of PCNA. *Nucleic Acids Res.* **35**, 6588–6597 (2007).
11. Bhagwat, M. & Nossal, N.G. Bacteriophage T4 RNase H removes both RNA primers and adjacent DNA from the 5′ end of lagging strand fragments. *J. Biol. Chem.* **276**, 28516–28524 (2001).
12. Stith, C.M., Sterling, J., Resnick, M.A., Gordenin, D.A. & Burgers, P.M. Flexibility of eukaryotic Okazaki fragment maturation through regulated strand displacement synthesis. *J. Biol. Chem.* **283**, 34129–34140 (2008).
13. Garg, P., Stith, C.M., Sabouri, N., Johansson, E. & Burgers, P.M. Idling by DNA polymerase delta maintains a ligatable nick during lagging-strand DNA replication. *Genes Dev.* **18**, 2764–2773 (2004).
14. Kang, Y.H., Lee, C.H. & Seo, Y.S. Dna2 on the road to Okazaki fragment processing and genome stability in eukaryotes. *Crit. Rev. Biochem. Mol. Biol.* **45**, 71–96 (2010).
15. Jin, Y.H. *et al.* The 3′→5′ exonuclease of DNA polymerase delta can substitute for the 5′ flap endonuclease Rad27/Fen1 in processing Okazaki fragments and preventing genome instability. *Proc. Natl. Acad. Sci. USA* **98**, 5122–5127 (2001).
16. Indiani, C., McInerney, P., Georgescu, R., Goodman, M.F. & O'Donnell, M. A sliding-clamp toolbelt binds high- and low-fidelity DNA polymerases simultaneously. *Mol. Cell* **19**, 805–815 (2005).
17. Kath, J.E. *et al.* Polymerase exchange on single DNA molecules reveals processivity clamp control of translesion synthesis. *Proc. Natl. Acad. Sci. USA* **111**, 7647–7652 (2014).
18. Beattie, T.R. & Bell, S.D. Coordination of multiple enzyme activities by a single PCNA in archaeal Okazaki fragment maturation. *EMBO J.* **31**, 1556–1567 (2012).
19. Dovrat, D., Stodola, J.L., Burgers, P.M. & Aharoni, A. Sequential switching of binding partners on PCNA during *in vitro* Okazaki fragment maturation. *Proc. Natl. Acad. Sci. USA* **111**, 14118–14123 (2014).
20. Dieckman, L.M., Johnson, R.E., Prakash, S. & Washington, M.T. Pre-steady state kinetic studies of the fidelity of nucleotide incorporation by yeast DNA polymerase delta. *Biochemistry* **49**, 7344–7350 (2010).
21. Ayyagari, R., Gomes, X.V., Gordenin, D.A. & Burgers, P.M. Okazaki fragment maturation in yeast. I. Distribution of functions between FEN1 AND DNA2. *J. Biol. Chem.* **278**, 1618–1625 (2003).
22. Johnson, K.A. Role of induced fit in enzyme specificity: a molecular forward/reverse switch. *J. Biol. Chem.* **283**, 26297–26301 (2008).
23. Burgers, P.M.J. *Saccharomyces cerevisiae* replication factor C. II. Formation and activity of complexes with the proliferating cell nuclear antigen and with DNA polymerases delta and epsilon. *J. Biol. Chem.* **266**, 22698–22706 (1991).
24. Langston, L.D. & O'Donnell, M. DNA polymerase delta is highly processive with proliferating cell nuclear antigen and undergoes collision release upon completing DNA. *J. Biol. Chem.* **283**, 29522–29531 (2008).
25. Nick McElhinny, S.A. *et al.* Abundant ribonucleotide incorporation into DNA by yeast replicative polymerases. *Proc. Natl. Acad. Sci. USA* **107**, 4949–4954 (2010).
26. Kunkel, T.A., Sabatino, R.D. & Bambara, R.A. Exonucleolytic proofreading by calf thymus DNA polymerase delta. *Proc. Natl. Acad. Sci. USA* **84**, 4865–4869 (1987).
27. Sparks, J.L. *et al.* RNase H2-initiated ribonucleotide excision repair. *Mol. Cell* **47**, 980–986 (2012).
28. Raghuraman, M.K. *et al.* Replication dynamics of the yeast genome. *Science* **294**, 115–121 (2001).
29. Podust, V.N., Podust, L.M., Müller, F. & Hübscher, U. DNA polymerase delta holoenzyme: action on single-stranded DNA and on double-stranded DNA in the presence of replicative DNA helicases. *Biochemistry* **34**, 5003–5010 (1995).
30. Sugimoto, N., Nakano, S., Yoneyama, M. & Honda, K. Improved thermodynamic parameters and helix initiation factor to predict stability of DNA duplexes. *Nucleic Acids Res.* **24**, 4501–4505 (1996).
31. Tsutakawa, S.E. *et al.* Human flap endonuclease structures, DNA double-base flipping, and a unified understanding of the FEN1 superfamily. *Cell* **145**, 198–211 (2011).
32. Kaiser, M.W. *et al.* A comparison of eubacterial and archaeal structure-specific 5′-exonucleases. *J. Biol. Chem.* **274**, 21387–21394 (1999).
33. Kao, H.I., Henricksen, L.A., Liu, Y. & Bambara, R.A. Cleavage specificity of *Saccharomyces cerevisiae* flap endonuclease 1 suggests a double-flap structure as the cellular substrate. *J. Biol. Chem.* **277**, 14379–14389 (2002).
34. Gomes, X.V. & Burgers, P.M.J. Two modes of FEN1 binding to PCNA regulated by DNA. *EMBO J.* **19**, 3811–3821 (2000).
35. Ganai, R.A., Osterman, P. & Johansson, E. Yeast DNA polymerase catalytic core and holoenzyme have comparable catalytic rates. *J. Biol. Chem.* **290**, 3825–3835 (2015).
36. Capson, T.L. *et al.* Kinetic characterization of the polymerase and exonuclease activities of the gene 43 protein of bacteriophage T4. *Biochemistry* **31**, 10984–10994 (1992).
37. Manosas, M. *et al.* Mechanism of strand displacement synthesis by DNA replicative polymerases. *Nucleic Acids Res.* **40**, 6174–6186 (2012).
38. Chapados, B.R. *et al.* Structural basis for FEN-1 substrate specificity and PCNA-mediated activation in DNA replication and repair. *Cell* **116**, 39–50 (2004).
39. Gary, R. *et al.* A novel role in DNA metabolism for the binding of Fen1/Rad27 to PCNA and implications for genetic risk. *Mol. Cell. Biol.* **19**, 5373–5382 (1999).
40. Jin, Y.H. *et al.* The multiple biological roles for the 3′→5′ exonuclease of *Saccharomyces cerevisiae* DNA polymerase delta require switching between the polymerase and exonuclease domains. *Mol. Cell. Biol.* **25**, 461–471 (2005).
41. Chabes, A. *et al.* Survival of DNA damage in yeast directly depends on increased dNTP levels allowed by relaxed feedback inhibition of ribonucleotide reductase. *Cell* **112**, 391–401 (2003).
42. Cannone, G., Xu, Y., Beattie, T.R., Bell, S.D. & Spagnolo, L. The architecture of an Okazaki fragment-processing holoenzyme from the archaeon *Sulfolobus solfataricus*. *Biochem. J.* **465**, 239–245 (2015).
43. Vijayakumar, S. *et al.* The C-terminal domain of yeast PCNA is required for physical and functional interactions with Cdc9 DNA ligase. *Nucleic Acids Res.* **35**, 1624–1637 (2007).
44. Montecucco, A. *et al.* DNA ligase I is recruited to sites of DNA replication by an interaction with proliferating cell nuclear antigen: identification of a common targeting mechanism for the assembly of replication factories. *EMBO J.* **17**, 3786–3795 (1998).
45. Smith, D.J. & Whitehouse, I. Intrinsic coupling of lagging-strand synthesis to chromatin assembly. *Nature* **483**, 434–438 (2012).

ONLINE METHODS

Proteins. RPA[46], PCNA[47], RFC[48], FEN1, and the PCNA-interaction-defective FEN1-p (F346G F347A)[34] were purified from *Escherichia coli* overexpression systems, whereas Pol δ and the exonuclease-defective Pol δ-DV (D520V) were purified from yeast overexpression systems[49].

DNA substrates. All oligonucleotides were obtained from Integrated DNA Technologies and were purified by either polyacrylamide gel electrophoresis or high-pressure liquid chromatography before use. Sequences of oligonucleotides are listed in **Supplementary Table 1**. Primer29, used in all studies, was either 5′-^{32}P-labeled with T4 polynucleotide kinase (New England BioLabs) and [γ-^{32}P]ATP, or was ordered with a 5′-Cy3 fluorophore. No difference in primer-extension activity was observed between the different labeling methods. Primer-extension DNA templates were generated by annealing labeled primer and blocking oligonucleotides to the template in a 0.8:2:1 ratio. 3′-labeled block templates were generated by annealing primer and labeled block to the template in a 1.4:0.8:1 ratio, respectively. 5′-labeled block templates were generated by annealing primer and labeled block to the template in a 0.8:1.4:1 ratio, respectively. To hybridize, oligonucleotides were heated to 75 °C in 100 mM NaCl and cooled slowly to room temperature. After hybridization, streptavidin was added in a two-fold molar excess to template–primer substrates. All substrates, except those in **Supplementary Figure 4i**, contain 3′- and 5′-biotin–streptavidin bumpers to support stable PCNA loading by RFC[21]. DNA concentrations in replication assays were calculated according to the labeled oligonucleotide concentration. In strand-displacement templates, the gap between the primer terminus and the 5′-block was limited to either two or five nucleotides to maximize the synchrony of replicating complexes initiating strand-displacement synthesis.

Replication reactions. All replication experiments were performed in a buffer containing 20 mM Tris-HCl, pH 7.8, 1 mM dithiothreitol, 200 μg/ml bovine serum albumin, 8 mM $Mg(OAc)_2$, and 100 mM NaCl. Unless otherwise noted, standard reaction conditions were 10 nM DNA template, 40 nM Pol δ (DV or wild type), 30 nM PCNA, 15 nM RFC, 100 μM α,β-methyleneadenosine 5′-triphosphate (AMP-CPP) for RFC-catalyzed loading of PCNA, and 50 nM RPA for studies in **Figure 1** or 25 nM RPA for all other studies. PCNA loading by RFC is an ATP-dependent process[9]. However, because ATP is also a substrate for Pol δ (ref. 25), it could not be used in our system. Therefore, we replaced ATP with AMP-CPP, which acts efficiently in PCNA loading but cannot be incorporated by the DNA polymerase. The Pol δ-DV (D520V) mutant was used in most reactions, unless otherwise noted. This exonuclease-deficient mutant prevents degradation of oligonucleotide substrates before reaction initiation[15].

Reactions were initiated with 250 μM of each dNTP, unless otherwise noted. In select experiments, physiological concentrations of the four dNTPs and rNTPs were used; physiological dNTP concentrations in *S. cerevisiae* were 16 μM dATP, 14 μM dCTP, 12 μM dGTP, and 30 μM dTTP, and the rNTP concentrations were 3 mM ATP, 0.5 mM CTP, 0.7 mM GTP, and 1.7 mM UTP[25].

All reactions except those in **Figure 5** and **Supplementary Figure 5** were performed in a quenched-flow apparatus (KinTek RQF-3) maintained at 30 °C with a circulating water bath. DNA templates were preincubated with Pol δ, with or without other protein factors (PCNA, RFC, and RPA) and AMP-CPP as indicated. The preassembled complexes were loaded into one loop of the quenched-flow apparatus. The second loop contained initiating nucleotides (and FEN1 when present) in reaction buffer. Reactions were initiated by mixture of equal volumes and quenched with 200 mM EDTA and 0.2% SDS. DNA products were ethanol-precipitated in the presence of 10 μg/ml glycogen and resolved on 12–20% denaturing polyacrylamide gels. Gels containing ^{32}P-labeled DNAs were dried and subjected to PhosphorImager analysis. Gels containing Cy3-labeled DNAs were visualized by detection of Cy3 fluorescence with a Typhoon-Trio (GE Healthcare). All quantifications were carried out with ImageQuant software (GE Healthcare).

Each reaction was performed at least twice under identical conditions. For exact repeats of strand-displacement reactions, variations in the fractional occupancy of specific products did not exceed 0.1, even at the shortest time points. At time points exceeding 50 ms, curves from identical replicates were indistinguishable. Observed rates in all figures are reported to highlight qualitative differences between reaction conditions, with standard errors reported for the fits of individual time courses.

Median analysis. The median analysis method was used to generate the data presented in **Figures 1e** and **4e** and **Supplementary Figures 1c,g** and **4h**. This methodology takes into consideration that complexes do not move with perfect synchrony through the available template, and it is described in detail in the legend to **Supplementary Figure 6**.

46. Henricksen, L.A., Umbricht, C.B. & Wold, M.S. Recombinant replication protein A: expression, complex formation, and functional characterization. *J. Biol. Chem.* **269**, 11121–11132 (1994).
47. Eissenberg, J.C., Ayyagari, R., Gomes, X.V. & Burgers, P.M. Mutations in yeast proliferating cell nuclear antigen define distinct sites for interaction with DNA polymerase delta and DNA polymerase epsilon. *Mol. Cell. Biol.* **17**, 6367–6378 (1997).
48. Gomes, X.V., Gary, S.L. & Burgers, P.M. Overproduction in *Escherichia coli* and characterization of yeast replication factor C lacking the ligase homology domain. *J. Biol. Chem.* **275**, 14541–14549 (2000).
49. Fortune, J.M., Stith, C.M., Kissling, G.E., Burgers, P.M. & Kunkel, T.A. RPA and PCNA suppress formation of large deletion errors by yeast DNA polymerase delta. *Nucleic Acids Res.* **34**, 4335–4341 (2006).

doi:10.1038/nsmb.3207

Erratum: Resolving individual steps of Okazaki-fragment maturation at a millisecond timescale

Joseph L Stodola & Peter M Burgers

***Nat. Struct. Mol. Biol.*; doi:10.1038/nsmb.3207; corrected online 19 April 2016**

In the version of this article initially published online, there were partial omissions within the schematics depicted in Figure 5a,b. These errors have been corrected for the print, HTML and PDF versions of the article.

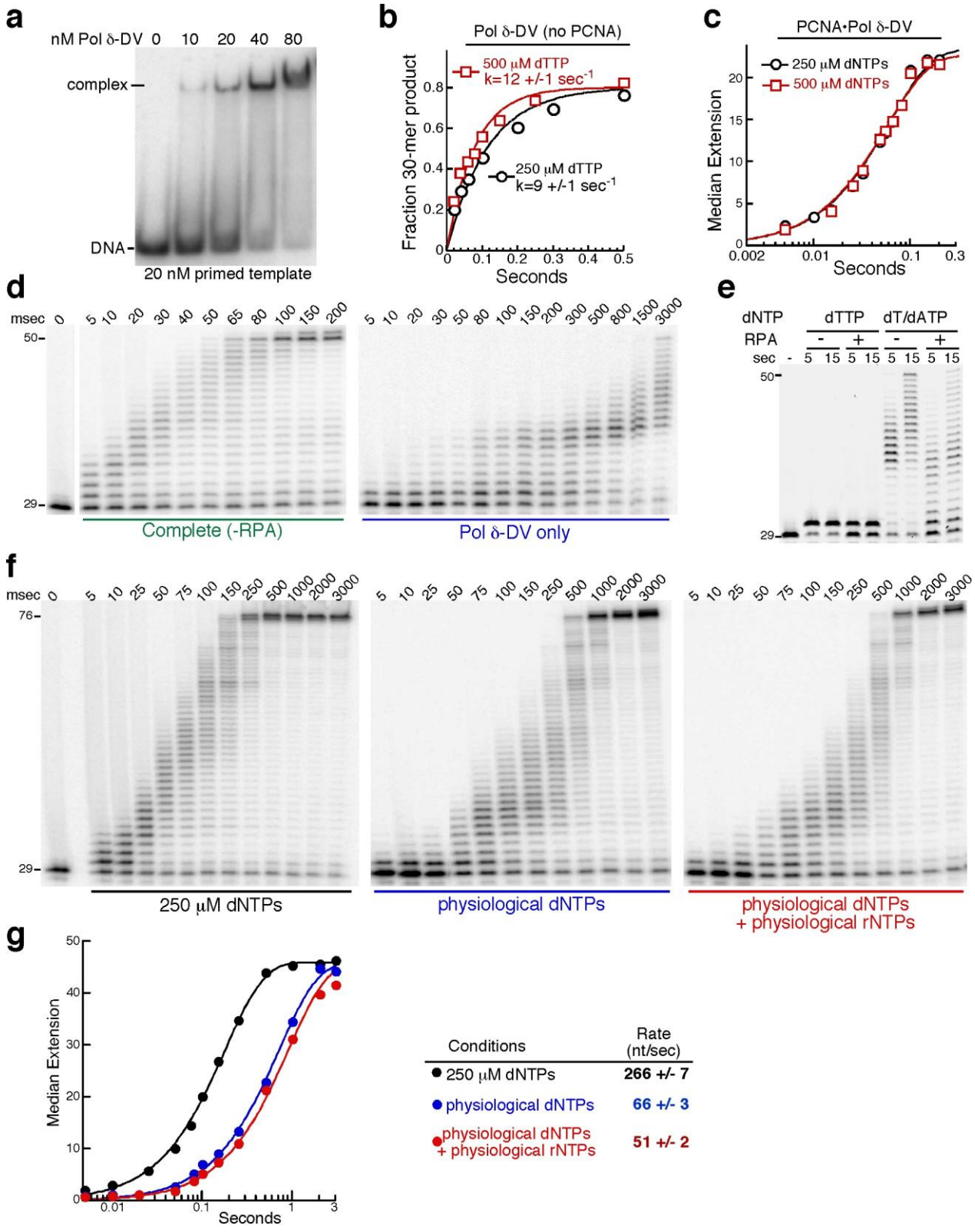

Supplementary Figure 1

Analysis of replication rates by Pol δ.

(a) Electrophoretic Mobility Shift Assay (EMSA) of Pol δ-DV binding to template-primer DNA (Fried, M. & Crothers, D.M. Equilibria and kinetics of lac repressor-operator interactions by polyacrylamide gel electrophoresis. *Nucleic Acids Res.* **9**, 6505-6518 (1981)). 20 nM DNA was incubated with increasing concentrations of Pol δ-DV. Complexes were resolved on a 5%, 1X TBE native polyacrylamide gel. Analysis was carried out with 20 nM template as this was the pre-incubation concentration of DNA prior to mixing with an equal volume of dNTP solution in the rapid-quench apparatus. (**b**) Single nucleotide incorporation by Pol δ-DV alone (no PCNA), identical to described in **Fig. 1 b,c**, with either 250 μM or 500 μM dTTP. Time courses were fit to single exponentials, representative of first-order kinetics. (**c**) Quantification of replication time courses of a homopolymeric DNA by PCNA-Pol δ. Experiments were performed identically to that in **Fig. 1d**, but with either 250 μM or 500 μM each of dTTP and dATP. Median analysis is described in detail in "Supplementary Experimental Procedures". (**d**) Replication through a homopolymeric stretch of DNA by PCNA-Pol δ; images of gels quantified in **Fig. 1e**. DNA template was pre-incubated with subsets of an enzyme mix containing Pol δ-DV, RPA, PCNA, RFC, and AMP-CPP. Omissions from this standard reaction mix are noted. Reactions were initiated with 250 μM dTTP and dATP each to allow extension of the 29-mer primer to a 50-mer product. (**e**) Effect of RPA on Pol δ-DV extension in the absence of PCNA. Primer extension reactions were performed on substrate described in **Fig. 1a**, with and without 50 nM RPA pre-bound to the single-stranded DNA template. Reactions were initiated with either 250 μM dATP or 250 μM each dATP and dTTP as noted. **(f)** Primer extension reactions by PCNA-Pol δ. Standard replication reactions on the template shown in **Fig. 1a** containing all components were initiated with either 250 μM each of all four dNTPs, all four dNTPs at *S. cerevisiae* physiological concentrations (16 μM dATP, 14 μM dCTP, 12 μM dGTP, 30 μM dTTP), or all four dNTPs and rNTPs at *S. cerevisiae* physiological concentrations (dNTPs as before plus 3 mM ATP, 0.5 mM CTP, 0.7 mM GTP, 1.7 mM UTP). **(g)** Quantification of data from **f**. The median extension product at each time point was determined and plotted as a function of time. Each curve was fit to a single exponential.

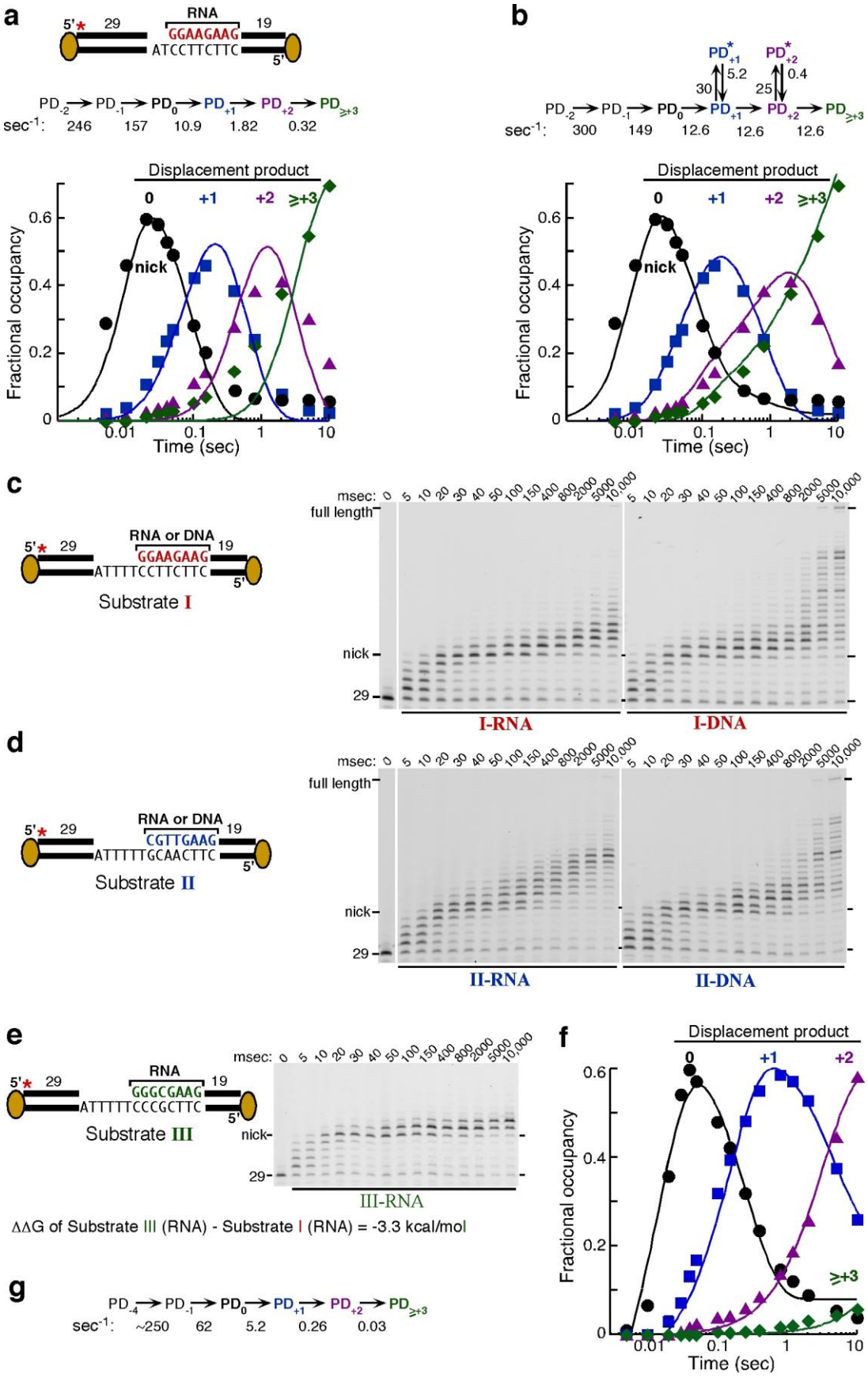
a
RNA
5'* 29
GGAAGAAG 19
ATCCTTCTTC
5'
PD-2 → PD-1 → PD0 → PD+1 → PD+2 → PD≥+3
sec-1: 246 157 10.9 1.82 0.32
Displacement product
0 +1 +2 ≥+3
nick
Fractional occupancy
Time (sec)
b
PD*+1 PD*+2
5.2 0.4
30 25
PD-2 → PD-1 → PD0 → PD+1 → PD+2 → PD≥+3
sec-1: 300 149 12.6 12.6 12.6
Displacement product
0 +1 +2 ≥+3
nick
Fractional occupancy
Time (sec)
c
RNA or DNA
5'* 29
GGAAGAAG 19
ATTTTCCTTCTTC
5'
Substrate I
msec: 0 5 10 20 30 40 50 100 150 400 800 2000 5000 10,000
full length
nick
29
I-RNA
I-DNA
d
RNA or DNA
5'* 29
CGTTGAAG 19
ATTTTTGCAACTTC
5'
Substrate II
msec: 0 5 10 20 30 40 50 100 150 400 800 2000 5000 10,000
full length
nick
29
II-RNA
II-DNA
e
RNA
5'* 29
GGGCGAAG 19
ATTTTTCCCGCTTC
5'
Substrate III
msec: 0 5 10 20 30 40 50 100 150 400 800 2000 5000 10,000
nick
29
III-RNA
ΔΔG of Substrate III (RNA) - Substrate I (RNA) = -3.3 kcal/mol
f
Displacement product
0 +1 +2
≥+3
Fractional occupancy
Time (sec)
g
PD-4 → PD-1 → PD0 → PD+1 → PD+2 → PD≥+3
sec-1: ~250 62 5.2 0.26 0.03

Supplementary Figure 2

Strand-displacement synthesis by exonuclease-deficient Pol δ.

(a, b) Global kinetic modeling of data from **Fig. 2a** to the respective kinetic models shown. KinTek Explorer software was used to perform fits (Johnson, K.A., Simpson, Z.B. & Blom, T. Global kinetic explorer: a new computer program for dynamic simulation and fitting of kinetic data. *Anal Biochem* **387**, 20-9 (2009)) The fitting shown in **Fig. 2b** was performed in a model-free manner, providing information concerning the observed macroscopic rates of strand displacement synthesis, but not about the molecular mechanism of the observed slow-down. In an attempt to better define this molecular mechanism, we performed global kinetic fitting of the data in **Fig. 2a** to two different models. First, we globally fit the data to the simplest model, in which the flap inhibits the actual rate of extension by Pol δ and a longer flap inhibits more effectively in **(a)**. This model yielded a poor fit, especially for the +2 and +3-nt displacement products. The rates obtained from this global fit were comparable to those generated by fitting each product curve to the sum of two exponentials individually (compare **(a)** with **Fig. 2b**). A second, more complex mechanism was considered, in which Pol δ equilibrates between two states during strand displacement, one that is competent for further extension and one incompetent for extension **(b)**. Fitting to such a model provided a better fit to the data, as is expected by the inclusion of more variables. Our modeling indicates that the incompetent state is not significantly populated during polymerization of single-strand DNA templates, but becomes increasingly more populated as strand displacement synthesis progresses. While several rates were not well defined by this model, we believe that its principle has merit because it provides a mechanistic explanation for Pol δ carrying out activities on flap substrates other than polymerization, such as idling and hand-off to FEN1. (**c, d**) Strand displacement time courses performed on the indicated Substrates I and II with either RNA or DNA-initiating blocking oligonucleotides. Select time points from these gels are shown in **Fig. 2b**. **(e)** Strand displacement time course performed on DNA Substrate III-RNA block. The reaction was performed identically to those in **(c)** and **(d)**. **(f)** Quantitation of data from **(e)**; Displacement products (0) and (+1) were fit to two exponentials, and (+2) and ($\geq$+3) to single exponentials. **(g)** Global KinTek modeling using the simple model in **(a)**. The experiments in **(e-g)** were carried out to show that the progressive slowdown observed during strand displacement synthesis in Substrates I and II was not the result of the specific DNA or RNA sequence used, but a consequence of the increasing length of the flap. In Substrate III, the dinucleotide stability for each pair of nucleotides within the four, 5'-proximal nucleotides was constant (5'-rGrGrGrC), yet the strand displacement time-course shows that rate of strand displacement synthesis progressively decreases as the nascent flap grows longer.

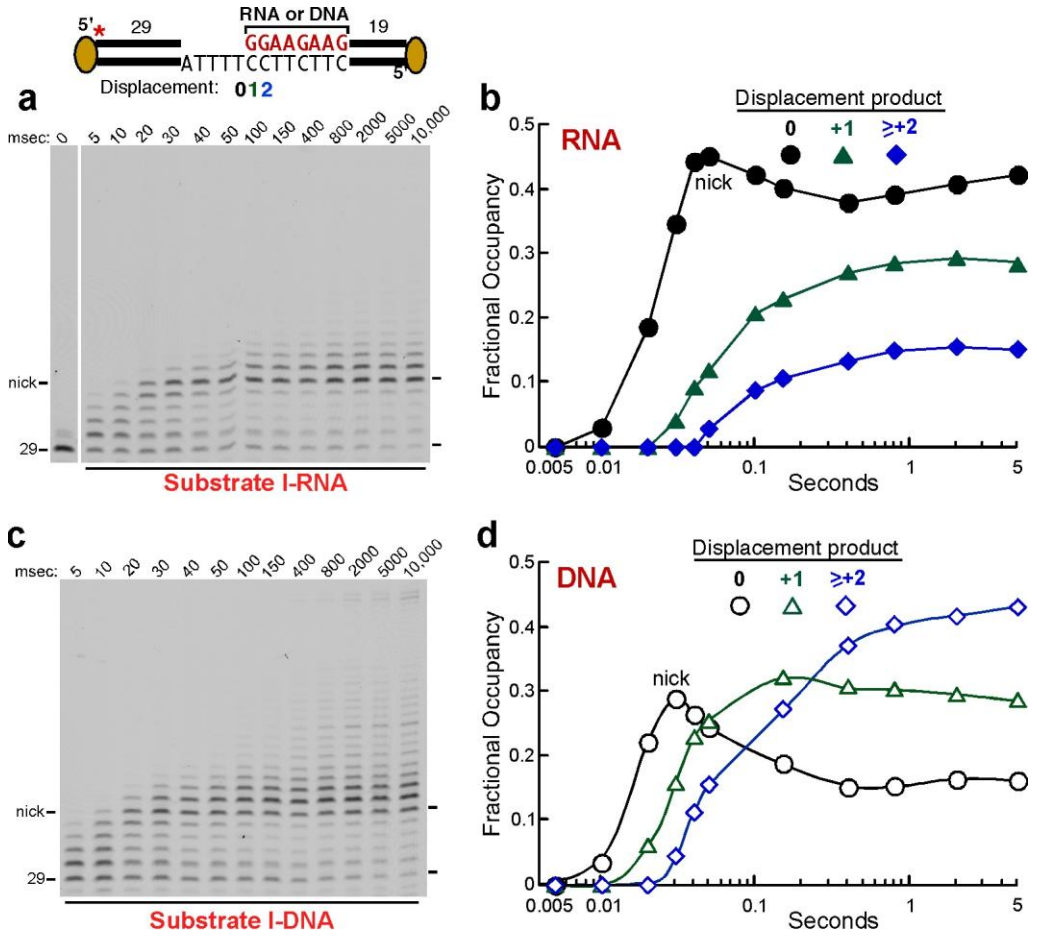

Supplementary Figure 3

Strand-displacement synthesis and idling by wild-type Pol δ.

(**a,c**) Strand displacement time courses performed with Pol δ-wt as described in **Fig. 3a**. The substrate and enzymes were pre-incubated in the presence of dCTP and dGTP to prevent polymerase degradation of the primer and blocking oligonucleotide. (**b,d**) Quantification of products in **a,c**. Fractional occupancy was determined and select products are plotted. The nick position product (0), +1 position past nick, and the +2 and greater position were plotted for both the RNA-initiating block (**a,b**) and the DNA block **(c,d)** of Substrate I. The **c** plot is also in Figure 3, but is shown again for easier comparison.

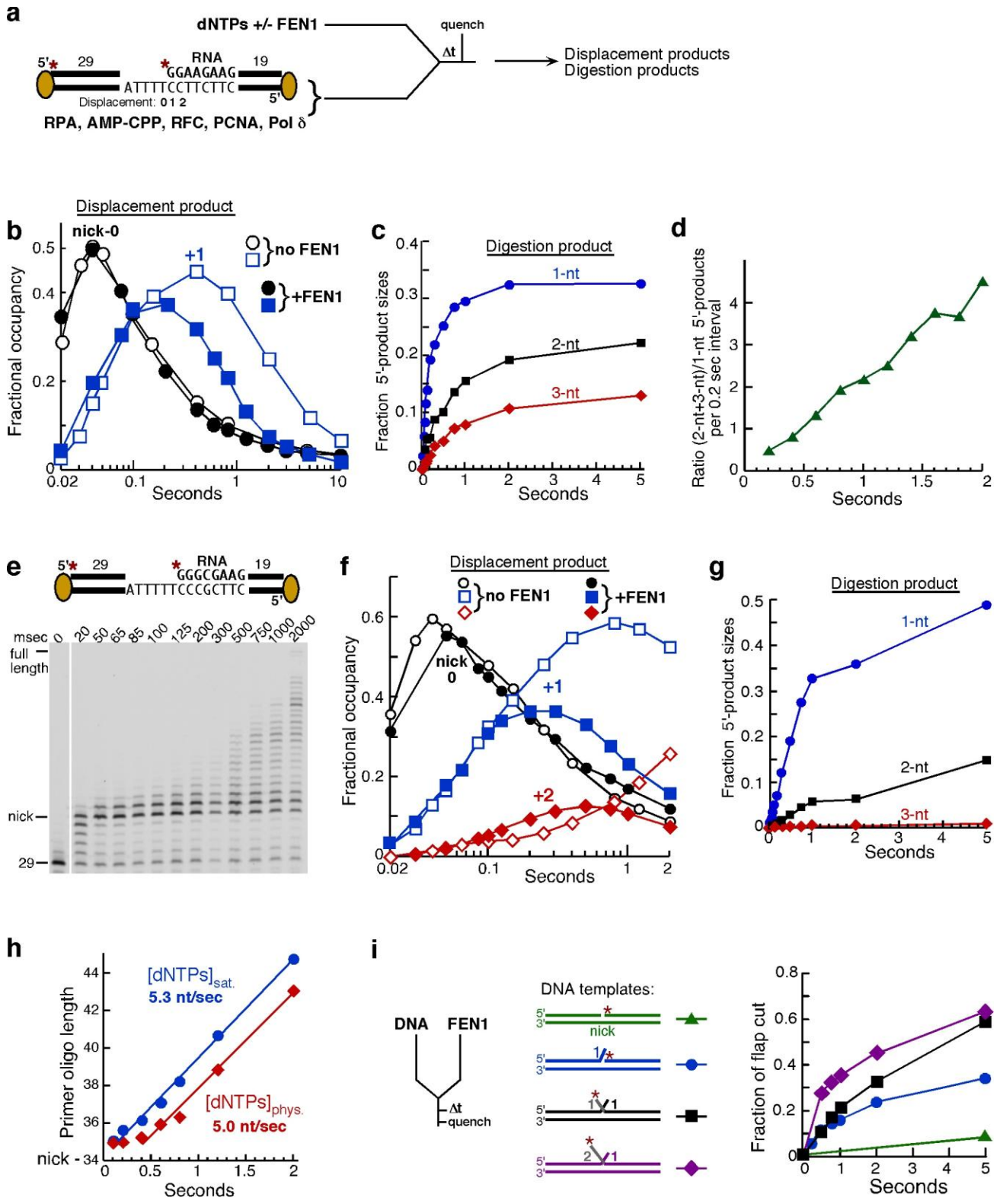

Supplementary Figure 4

Nick translation by Pol δ and FEN1.

(**a**) Experimental design of nick translation assay. (**b**) Quantification of data from **Fig. 2d** (no FEN1) and **Fig. 4b**, top panel (+FEN1),

showing nick position and +1 displacement product. (**c**) FEN1-cut products from Substrate I-RNA with 5'-labeled blocking oligonucleotide. The fraction of each product size is shown. The total of cut products and substrate remaining equals 1. (**d**) The ratio of (2-nt + 3-nt)/1-nt product formed during each subsequent 0.2 sec interval was plotted against assay time. The plot shows that at the start the 1-nt product predominated (ratio =0.3), while after 2 sec, the larger products predominated (ratio =4.5). (**e**) Nick translation assay on Substrate III-RNA block, as diagramed in **a**. (**f**) Quantification of **e** (+FEN1) and **Supplementary Fig. 2e (**no FEN1). Nick position (0), and +1 and +2 displacement products were plotted. (**g**) FEN1-cut products from Substrate III-RNA with 5'-labeled blocking oligonucleotide. The fraction of each product size is shown. The total of cut products and substrate remaining equals 1. (**h**) Median extension analysis of nick translation assays performed at 250 μM each dNTP (blue), and at physiological dNTP levels (red, concentrations listed in legend to **Supplementary Fig. 1f**). Data for saturating dNTPs are the same as in **Fig. 4e**. Data collected with low dNTP levels shows a lag in nick translation at early time points, which we attribute to slower gap filling and formation of the +1 flap at the lower, physiological dNTPs. Comparison of the two slopes in the linear range indicates that iterative nick translation proceeds at approximately the same rate at physiological as at saturating nucleotide concentrations. (**i**) Quench-flow assay with FEN1 and various flap-containing DNAs. Reactions were initiated by mixing FEN1 with DNA template. Other than the nick-containing template (green), DNAs contained a single extrahelical 3'-nucleotide complementary to the template. Templates then contained either 0 (blue), 1 (black), or 2 (purple) extrahelical 5'-rU bases, not complementary to the template. All templates were labeled with a 5'-^{32}P on the strand cut by FEN1. The fraction of flap cut is plotted. These assays were carried out without PCNA since it was not efficiently loaded on the flap substrates.

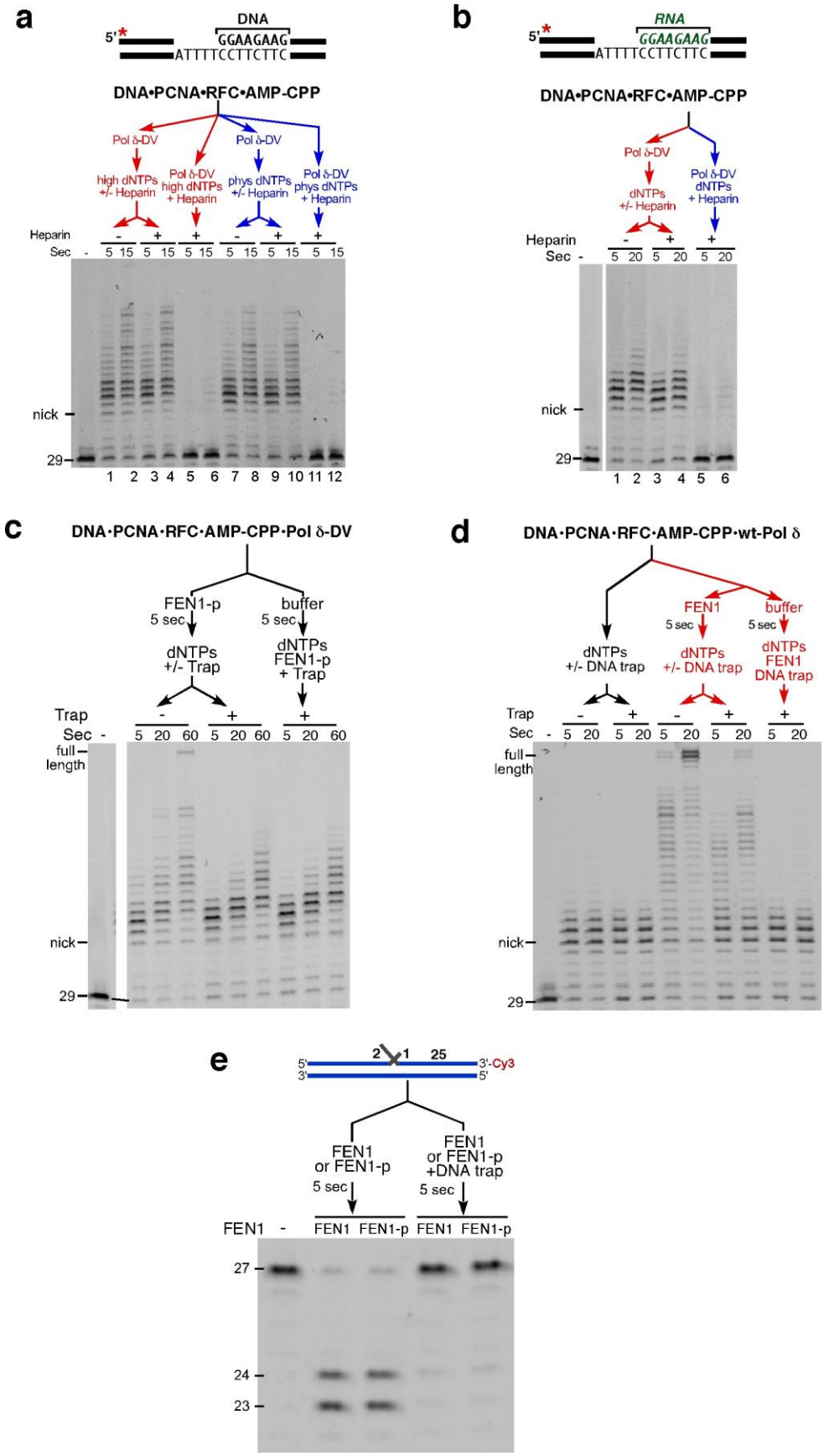
a
DNA
5'*
GGAAGAAG
ATTTTCCTTCTTC
DNA•PCNA•RFC•AMP-CPP
Pol δ-DV
Pol δ-DV
high dNTPs +/- Heparin
Pol δ-DV high dNTPs + Heparin
phys dNTPs +/- Heparin
Pol δ-DV phys dNTPs + Heparin
Heparin
Sec - 5 15 5 15 5 15 5 15 5 15 5 15
nick
29
1 2 3 4 5 6 7 8 9 10 11 12
b
RNA
5'*
GGAAGAAG
ATTTTCCTTCTTC
DNA•PCNA•RFC•AMP-CPP
Pol δ-DV
Pol δ-DV
dNTPs +/- Heparin
dNTPs + Heparin
Heparin
Sec - 5 20 5 20 5 20
nick
29
1 2 3 4 5 6
c
DNA•PCNA•RFC•AMP-CPP•Pol δ-DV
FEN1-p 5 sec
buffer 5 sec
dNTPs +/- Trap
dNTPs FEN1-p + Trap
Trap
Sec - 5 20 60 5 20 60 5 20 60
full length
nick
29
d
DNA•PCNA•RFC•AMP-CPP•wt-Pol δ
FEN1 5 sec
buffer 5 sec
dNTPs +/- DNA trap
dNTPs +/- DNA trap
dNTPs FEN1 DNA trap
Trap
Sec - 5 20 5 20 5 20 5 20 5 20
full length
nick
29
e
2 1 25
5'
3'
3'-Cy3
5'
FEN1 or FEN1-p 5 sec
FEN1 or FEN1-p +DNA trap 5 sec
FEN1 - FEN1 FEN1-p FEN1 FEN1-p
27
24
23

Supplementary Figure 5

Processivity of the nick-translation machinery.

(**a**) Similar to **Fig. 5a**; strand displacement time-course by PCNA-Pol δ on Substrate I-DNA block. Standard reaction conditions were used, initiated with either 250 μM of each dNTP (high) or physiological levels of each dNTP (phys, concentrations listed in legend to **Supplementary Fig. 1f**). 10 μg/ml heparin was used as trap for free Pol δ-DV in noted lanes. (**b**) Similar to **Supplementary Fig. 5a**, lanes 1-6 (250 μM each dNTP), except Substrate I-RNA block was used instead of a DNA-block. (**c**) Companion to **Fig. 5b**; nick translation assay with forced single turnover of 40 nM FEN1-p, containing mutations in the FEN1 PIP-motif. DNA template was Substrate I-RNA block. Reactions were initiated with 250 μM each dNTP with or without 6 μM oligonucleotide FEN1 trap to trap free FEN1-p. The data show that the trap completely blocked FEN1-p action, even when it was pre-bound to the DNA-PCNA- Pol δ complex, indicating that it is not stably associated with this complex. (**d**) Nick translation assay with forced single turnover of 40 nM FEN1, with wild-type Pol δ. Reactions were initiated with 250 μM each dNTP with or without 6 μM oligonucleotide FEN1 trap to trap free FEN1. The data show that FEN1 is able to remain associated with the PCNA-wild-type Pol δ complex throughout nick translation (**e**) Testing the efficiency of the FEN1 oligonucleotide trap; FEN1 and FEN1-p cutting of labeled substrate containing a stable flap. Labeled DNA contained a single nucleotide 3'-flap and a two-nucleotide 5'-flap (both non-complementary to template), with a 3'-Cy3 label on the strand cut by FEN1. Reactions were initiated by mixing the enzyme with DNA template. To test the effectiveness of the oligonucleotide trap, FEN1 and FEN1-p were pre-incubated with excess trap template prior to incubation with labeled template. The structure of the trap substrate was identical to that of the labeled substrate.

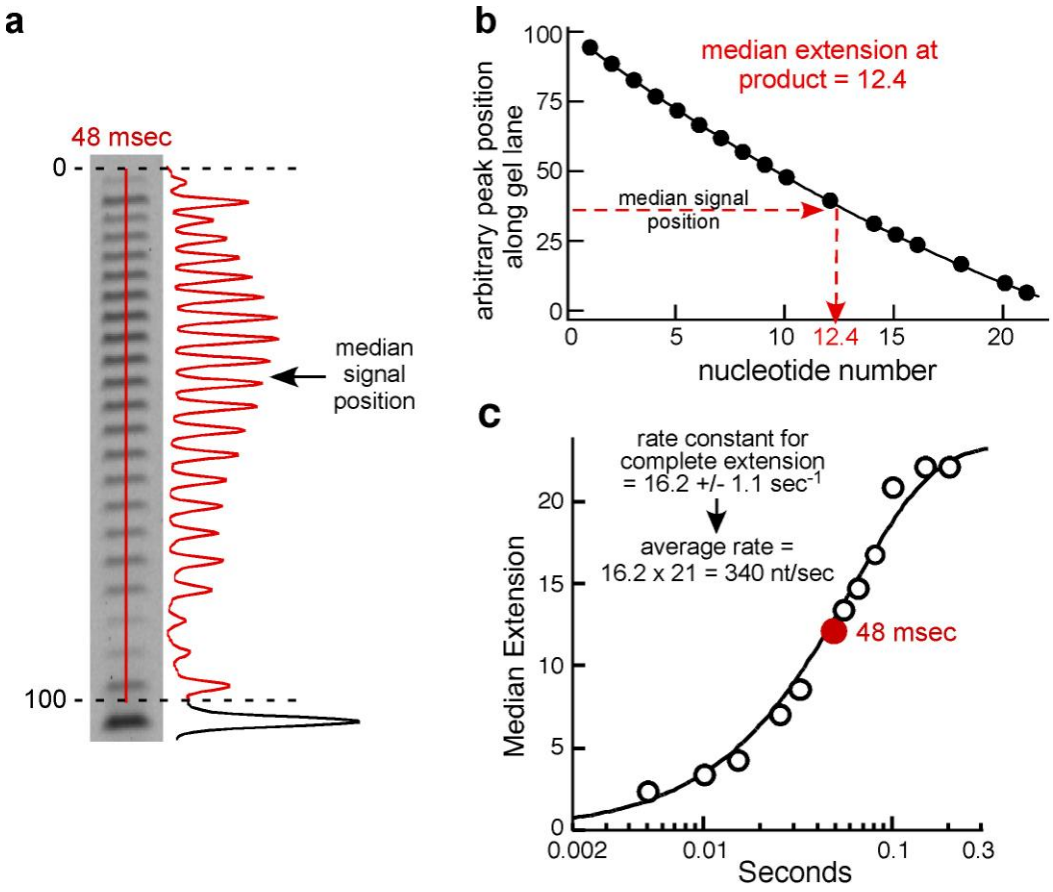

Supplementary Figure 6

Median analysis of replication rates.

This analysis method was used to generate the data presented in **Fig. 1e, 4e**, and **Supplementary Fig. 1c,g, 4h**. **(a)** Plot profiles of all products, except starting material, were produced using ImageQuant (GE Healthcare). These profiles plotted the intensity signal in the gel against an arbitrary y-coordinate. Following background subtraction, we determined the position on the y-coordinate at which the median of the total lane signal was. This was defined as the point along the lane coordinate in which 50% of the signal in which 50% of the signal lay above and below. **(b)** Next, for each gel, a standard curve was produced, fit to a quadratic function, in order to convert the arbitrary y-coordinate values to a value represented in nucleotides. **(c)** After determining the median product for many points throughout an entire time-course, the plots were assembled.

Supplementary Table. Oligonucleotides used in this study

Primer29	5'-TCA GCG CGA GCA TGA CAT TGA AGG TAA CC-3'
Primer29-Cy3	5'-Cy3-TCA GCG CGA GCA TGA CAT TGA AGG TAA CC-3'
Template-AT_{20}	5'-BiotinTEG-TTC CTT CAA CCA GCT TAC CTT CTT CCT TTT TTT TTT TTT TTT TTT TAG GTT ACC TTC AAT GTC ATG CTC GCG CTG A-BiotinTEG-3'
Template-Sub I	5'-BiotinTEG-TCT TCC TTC AAC CAG CTT ACC TTC TTC CTT TTA GGT TAC CTT CAA TGT CAT GCT CGC GCT GA-BiotinTEG-3'
Block-Sub I-pRNA	5'-Phos-GGA AGA AGG TAA GCT GGT TGA AGG AAG-3'
Block-Sub I-pDNA	5'-Phos-rGrGrA rArGrA rArGG TAA GCT GGT TGA AGG AAG-3'
Template-Sub II	5'-BiotinTEG-TCT TCC TTC AAC CAG CTT ACC TTC AAC GTT TTA GGT TAC CTT CAA TGT CAT GCT CGC GCT GA-BiotinTEG-3'
Block-Sub II-pDNA	5'-Phos-CGT TGA AGG TAA GCT GGT TGA AGG AAG-3'
Block-Sub II-pRNA	5'-Phos-rCrGrU rUrGrA rArGG TAA GCT GGT TGA AGG AAG-3'
Template-Sub III	5'-BiotinTEG-TCT TCC TTC AAC CAG CTT ACC TTC GCC CTT TTA GGT TAC CTT CAA TGT CAT GCT CGC GCT GA-BiotinTEG-3'
Block-Sub III-pRNA	5'-Phos-rGrGrG rCrGrA rArGG TAA GCT GGT TGA AGG AAG-3'
Block-Sub I-pRNA-3'Cy3	5'-Phos-rGrGrA rArGrA rArGG TAA GCT GGT TGA AGG AAG-Cy3-3'
Block-Sub I-RNA	5'-rGrGrA rArGrA rArGG TAA GCT GGT TGA AGG AAG-3'
Block-Sub III-RNA	5'-rGrGrG rCrGrA rArGG TAA GCT GGT TGA AGG AAG-3'
FEN1 trap template	5'-TCT TCC TTC AAC CAG CTT ACC TTC TTC CTT TTA GGT TAC CTT CAA TGT CAT GCT CGC GCT GA-3'
FEN1 trap|3'-flap	5'-TCA GCG CGA GCA TGA CAT TGA AGG TAA CCT AAA AT-3'
FEN1 trap|5'-flap	5'-TT GGA AGA AGG TAA GCT GGT TGA AGG AAG-3'
FEN1 template-nick primer	5'-TCA GCG CGA GCA TGA CAT TGA AGG TAA CCT AAA A-3'
FEN1 template-3'G primer	5'-TCA GCG CGA GCA TGA CAT TGA AGG TAA CCT AAA AG-3'
FEN1-template-U1 block	5'-rU rGrGrA rArGrA rArGG TAA GCT GGT TGA AGG AAG-3'
FEN1-template-U2 block	5'-rUrU rGrGrA rArGrA rArGG TAA GCT GGT TGA AGG AAG-3'